Cylindrical model of a helicon-generated plasma

IEPC-2009-193

Presented at the 31st International Electric Propulsion Conference,
University of Michigan, Ann Arbor, Michigan, USA
September 20–24, 2009

Eduardo Ahedo *
Universidad Politécnica de Madrid, Madrid 28040, Spain

A two-dimensional, variable-separation model of the plasma dynamics inside a cylindrical chamber with an axial magnetic field is derived. The energy absorbed from an helicon-wave ionizes the injected gas and heats the plasma. The magnetic field is found to provide a good radial confinement of the plasma leading to negligible current and power losses to the lateral wall. An efficiency study aimed at a thruster application of the device is carried out, in terms of magnetic field, absorbed power, and injected flow. Losses to the rear-wall are a serious concern in the selected configuration, leading to a fall of internal efficiency, i.e. the ratio of plasma-beam power at the chamber exit to absorbed power, to values below a 40%.

I. Introduction

A helicon thruster is constituted of an helicon source for plasma generation and heating, and a magnetic nozzle for plasma acceleration.[1,2] The helicon source is constituted of a long dielectric cylinder with an open front end E, a gas injection system (usually at the rear wall A of the chamber), an applied axial magnetic field, and an antenna that emits helicon waves.[3] Wave energy is deposited into the plasma via plasma-wave resonance. Heated electrons ionize the injected the neutral gas by bombardment. The applied magnetic field has a double role: to enhance wave energy deposition (by operation in the efficient 'blue mode') and to confine the plasma plasma around the axis of the chamber, thus reducing the losses to the lateral walls and producing a highly collimated beam. For instance, Tysk et al.[4] find a 50 times radial decrease of the plasma density (for a 1000G field), instead of the 1.6 times decrease in a free-acceleration unmagnetized presheath. Strong radial decreases of n_e are also found by Gilland et al.[5]

For an efficient operation of the helicon thruster, most of the gas injected must be ionized, which means a strong depletion of the neutral gas density along the cylindrical chamber. Thanks to the self-induced electric field the created plasma flows towards the chamber front exit E and then expands outside in the magnetic nozzle. In general, the throat of the magnetic nozzle is located near that exit so that the plasma is expected to reach sonic conditions there. The electron population is confined by the electric potential profile, except for the small electron current needed to keep the plasma current-free.

Plasma physics in an axisymmetric helicon thruster consists of three coupled stages: (1) wave-plasma resonance and energy deposition physics, (2) plasma dynamics inside the chamber, and (3) plasma dynamics in the divergent magnetic nozzle. Stages (1) and (2) are strongly coupled but, since they take place in different time scales, they can be studied separately if the plasma density profile, $n(r,z)$, and the absorbed power density $P_a(r,z)$, are taken as input for the wave-plasma resonance and the internal dynamics models, respectively.[6] Stage (2) and (3) are matched around the chamber exit E. This paper formulates a two-dimensional(2D) fluid model of stage (2). Plasma supersonic expansion in the magnetic nozzle is treated in Refs. 7, 8.

The 2D model is based on decoupling partially the radial and axial dynamics, making use of an approximate variable-separation technique implemented successfully by Ahedo et al.[9] for the plasma discharge in a Hall thruster. There, the main coupling parameter between the axial and radial models is the local

*Professor. E-mail: eduardo.ahedo@upm.es. Full address: E.T.S. Ingenieros Aeronáuticos, Plaza Cardenal Cisneros, Madrid 28040

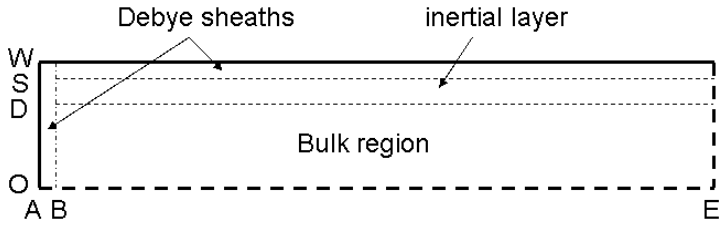

Figure 1. Sketch of the plasma regions in the chamber.

wall-recombination frequency. Fruchtman et al.[10] have applied a similar technique to the plasma discharge in a helicon source. In their model: (a) the neutral density is taken constant, i.e. $n_n(z) = \text{const}$, (b) the axial response is postulated symmetric with respect to the chamber central radial section, (c) ion-neutral (i-n) collision effects on ions are considered a central phenomenon; (d) and electron dynamics are purely diffusive. In the model proposed here the depletion of the injected neutral gas is taken into account in order to determine the propellant utilization. As a consequence, the plasma response at the chamber upstream and downstream half-regions is asymmetric. Then, recent results by Ahedo[11] on the 1D radial dynamics of a magnetized plasma in an infinite cylinder will be used. That work, which extends classical ones by Tonks[12] and Ewald et al.[13] and a recent one by Sternberg et al.,[14] stand out the role of the azimuthal electron inertia in the radial plasma structure. The main results of that work which are of application here are the following:

1. In the magnetized regime, the radial quasineutral structure consists of a bulk diffusive region plus a thin inertial layer, of a thickness about a local electron gyroradius;
2. The transition between the two regions occurs when the electron azimuthal velocity is of the order of the electron thermal velocity, $c_e = \sqrt{T_e/m_e}$;
3. Plasma pressure in the bulk region is balanced by the magnetic confinement force, whereas the electric force is much smaller;
4. The ion azimuthal drift is negligible always;
5. Azimuthal electron inertia effects are dominant in the inertial layer;
6. The inertial layer provides the correct value of the electron azimuthal energy that is later lost at the wall by collected electrons;
7. There exist analytical asymptotic solutions for the bulk region and the inertial layer.

The analytical solution of the 1D radial model will be postulated here as the radial dependence of the 2D model. Then, the 1D model for the axial variation will be formulated and analyzed. Fruchtman et al. assume that the electron temperature T_e is constant and determine it from a global energy balance. The same approach will be followed here. A constant T_e hypothesis is supported experimentally by Gilland et al.[5] In any case, a reliable solution of T_e from an energy equation depends heavily on the spatial distribution of the absorbed power, $P_a(r, z)$, that is on the coupling with the plasma-wave resonance model.

This work pretends to provide theoretical support to an European project aimed at developing a small helicon thruster.[15]

II. Model formulation

We consider a steady-state, cylindrical model of a plasma inside a chamber of radius R and length L. Figure 1 sketches the different plasma regions inside the chamber. For sake of convenience the velocity vectors of the different species are expressed as

$$\boldsymbol{u} + u_\theta \mathbf{1}_\theta,$$

Chamber radius	R	1cm
Chamber length	L	10cm
Mass flow	$\dot{m}$	0.1 mg/s
Current at full ionization	I_m	0.24A
Neutral velocity	u_n	310 m/s
Neutral density	n_{n0}	$1.5 \cdot 10^{19}\mathrm{m}^{-3}$
Plasma density	n_0	$10^{18}\mathrm{m}^{-3}$
Plasma temperature	T_e	10eV
Magnetic field	B	1000G
sound velocity	c_s	$4.9 \cdot 10^3\mathrm{m/s}$
thermal velocity	c_e	$1.3 \cdot 10^6\mathrm{m/s}$
Alfven velocity	c_A	$3.5 \cdot 10^5\mathrm{m/s}$
Debye length	λ_d	$2.4 \cdot 10^{-2}\mathrm{mm}$
electron Larmor radius	l_e	$7.5 \cdot 10^{-2}\mathrm{mm}$
ion Larmor radius	l_i	$20 \cdot 10^{-2}\mathrm{mm}$
ionization mean-free-path	λ_0	2.1cm
ionization rate	R_{ion}	$1.5 \cdot 10^{-14}\mathrm{m}^3/\mathrm{s}$
e-n collision rate	R_{en}	$3.2 \cdot 10^{-13}\mathrm{m}^3/\mathrm{s}$
i-n CEX rate (based on $c_{in} \approx c_s$)	R_{in}	$9.3 \cdot 10^{-16}\mathrm{m}^3/\mathrm{s}$
e-i collision rate	R_{ei}	$1.2 \cdot 10^{-12}\mathrm{m}^3/\mathrm{s}$
lower-hybrid frequency	ω_{lh}	$6.5 \cdot 10^7\mathrm{s}^{-1}$
radial transit frequency	c_s/R	$4.9 \cdot 10^5\mathrm{s}^{-1}$
ionization frequency	ν_{ion}, ν_0	$2.3 \cdot 10^5\mathrm{s}^{-1}$
e-n collision frequency	ν_{en}	$4.9 \cdot 10^6\mathrm{s}^{-1}$
i-n collision frequency (n on i)	ν_{in}	$1.4 \cdot 10^4\mathrm{s}^{-1}$
e-i collision frequency (i on e)	ν_{ei}	$1.1 \cdot 10^6\mathrm{s}^{-1}$

Table 1. Typical plasma parameters for a small helicon source operating on Argon; $\ln\Lambda = 12.5$**.**

with $\boldsymbol{u} = u_r\mathbf{1}_r + u_z\mathbf{1}_z$ representing only the velocity longitudinal component. We assume: an axisymmetric plasma response; plasma quasineutrality, $n_e = n_i$, except for the Debye sheaths; a constant axial magnetic field, $\boldsymbol{B} = B\mathbf{1}_z$; a negligible azimuthal velocity of ions;[11] negligible longitudinal components of electron inertia, $m_e\boldsymbol{u}_e \cdot \nabla\boldsymbol{u}_e \ll \nabla p_e$; negligible ion pressure; constant electron temperature, $T_e = \text{const}$; and a low-enough neutral velocity, $u_n \ll u_i$.

Then, the continuity equations are

$$\nabla \cdot n_e\boldsymbol{u}_i = \nabla \cdot n_e\boldsymbol{u}_e = -\nabla \cdot n_n\boldsymbol{u}_n = n_e n_n R_{ion}. \tag{1}$$

Using these equations the momentum equations for ions and electrons become

$$m_i n_e \boldsymbol{u}_i \cdot \nabla\boldsymbol{u}_i = -en_e\nabla\phi - m_i n_e(\nu_i\boldsymbol{u}_i + \nu_{in}\boldsymbol{u}_n), \tag{2}$$

$$0 = -T_e\nabla n_e + en_e\nabla\phi - en_e Bu_\theta\mathbf{1}_r + m_e n_e\left(-\nu_e\boldsymbol{u}_e + \nu_{ei}\boldsymbol{u}_i + \frac{u_\theta^2}{r}\mathbf{1}_r\right), \tag{3}$$

$$m_e n_e \boldsymbol{u}_e \cdot \nabla u_\theta = eBn_e u_{re} - m_e n_e\left(\nu_e u_\theta + \frac{u_\theta u_{re}}{r}\right). \tag{4}$$

Here: u_θ is the electron azimuthal velocity; $m_e/m_i \ll 1$ and $u_n \ll u_i$ has been used to simplify some equations;

$$\nu_e(r,z) = \nu_{ion} + \nu_{en} + \nu_{ei}, \qquad \nu_i(r,z) = \nu_{ion} + \nu_{in} + \nu_{ei}m_e/m_i \tag{5}$$

are the effective collision frequencies for ions and electrons, respectively, with contributions from ionization, $\nu_{ion} = n_n R_{ion}(T_e)$, electron-neutral(e-n) collisions, $\nu_{en} = n_n R_{en}(T_e)$, ion-neutral(i-n) collisions,

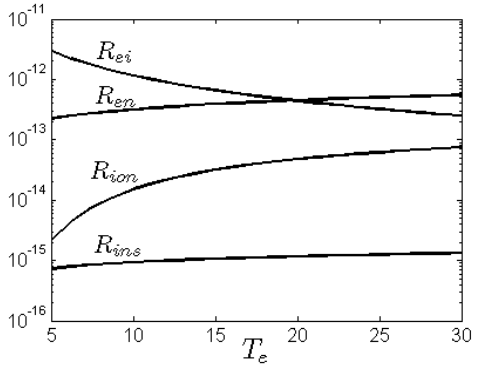

Figure 2. Collisional rates versus plasma temperature; $n_e = 10^{18}\mathbf{m}^{-3}$ was used for $\ln\Lambda$ in R_{ei}.

$\nu_{in} = n_n R_{in}(c_{in})$, with $c_{in} = |\boldsymbol{u}_i - \boldsymbol{u}_n|$, and electron-ion (e-i) collisions, $\nu_{ei} = n_e R_{ei}(T_e, n_e)$. The Appendix provides expressions for the different collision rates and Fig. 2 depicts them for argon. Neutral dynamics are an auxiliary aspect of this model and a detailed model of them is out of the scope of this work. A simple model for $\boldsymbol{u}_n$ will be selected later. Table 1 gives typical values of plasma magnitudes for the small helicon thruster.[15]

A. The radial structure

Let us consider that, first, the cylinder is long enough (i.e. $L \gg R$) so that axial gradients are much smaller than radial ones and, second, the plasma is within the parametric region

$$c_s/R \ll \nu_e \ll \omega_{lh}, \tag{6}$$

with $c_s = \sqrt{T_e/m_i}$ the sound speed and $\omega_{lh} = eB/\sqrt{m_e m_i}$ the lower-hybrid frequency. This parametric region corresponds to the main magnetized regime of the radial model of Ahedo.[11] Assuming longitudinal-current ambipolarity,

$$\boldsymbol{u}_e = \boldsymbol{u}_i, \tag{7}$$

and making use of the known analytical solutions for the radial bulk region,[11–13] plasma variables are assumed to behave in the following way:

$$n_e(r,z) = n_e(0,z) J_0\left(a_0 \frac{r}{R}\right), \quad u_\theta(r) = c_e \delta \frac{J_1(a_0 r/R)}{J_0(a_0 r/R)}, \quad u_r(r,z) = \frac{\nu_e}{\omega_{ce}} u_\theta(r), \quad u_z = u_z(z), \tag{8}$$

with J_0 and J_1 Bessel functions of the first kind, $a_0 \simeq 2.405$ the first zero of J_0, and

$$\delta = \ell_e/R \equiv c_s/(R\omega_{lh})$$

the relative electron gyroradius, which is a measure of the radial magnetic confinement.

Figure 3 shows the bulk part of the radial solution, which is is valid up to $r/R \sim 1 - \delta$. Then there is the inertial layer, but its detailed structure can be ignored here. Notice that $u_{\theta e}$ grows very steeply near the transition to the inertial layer.

III. Axial dynamics

The axial model is obtained as the radially-averaged approximation of the 2D fluid equations and works with plasma variables that depend only on z. Using Eq. (8) and taking

$$n(z) = \frac{2}{R^2}\int_0^R dr\ r n_e(r,z) \simeq \frac{n_e(0,z)}{2.3} \tag{9}$$

as the r-averaged plasma density, and assuming a simple advection model for neutrals with $n_n = n_n(z)$, $\boldsymbol{u}_n = u_n \mathbf{1}_z$, and $u_n = \text{const} \ll u_z$, the axial equations are

$$\frac{d}{dz}(n u_z) = -u_n \frac{dn_n}{dz} = n(\nu_{ion} - \nu_w), \tag{10}$$

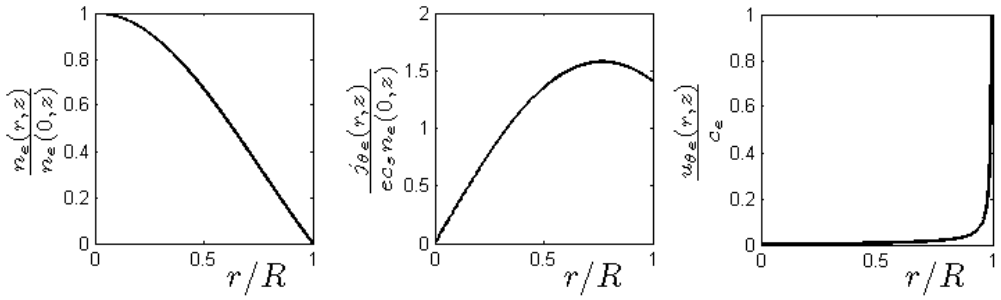

Figure 3. Radial profiles for $\delta = 0.01$.

$$\frac{1}{n}\frac{d}{dz}(nu_z^2) = -\frac{e}{m_i}\frac{d\phi}{dz} - (\nu_{in} + \nu_w)u_z + \nu_{ion}u_n, \tag{11}$$

$$0 = \frac{d}{dz}\left(e\phi - T_e \ln n\right), \tag{12}$$

where: the small axial resistivity of electrons has been neglected; all frequency expressions are assumed to depend on z only; and

$$n\nu_w = 2n_{eS}c_s/R \tag{13}$$

accounts for the plasma recombination at the lateral wall.

The ion and neutral conservation equations yield

$$n_n u_n + n u_z = g_0, \tag{14}$$

with $g_0 = \dot{m}/(\pi R^2 m_i) = \text{const}$ and $\dot{m}$ the particle flux and the injected mass flow. Manipulating Eqs. (10)- (12), one obtains

$$(c_s^2 - u_z^2)\frac{du_z}{dz} = [(\nu_{ion} + \nu_{in})u_z^2 + (\nu_{ion} - \nu_w)c_s^2], \tag{15}$$

$$(c_s^2 - u_z^2)\frac{dn}{dz} = -u_{zi}n(2\nu_{ion} + \nu_{in} - \nu_w), \tag{16}$$

as the differential set to integrate, with singularities at $u_z = \pm c_s$. Algebraic equations (12) and (14) yield ϕ and n_n.

Figure 2 shows that the ratio $\nu_{in}/\nu_{ion} = R_{in}/R_{ion}$ is small for the range of T_e of interest: one has $\nu_{in}(c_s)/\nu_{ion} = R_{in}(c_s)/R_{ion} < 0.1$ for $T_e >$8eV. Therefore, i-n collisions have a marginal role in the plasma axial dynamics and can be disregarded in the analysis of the axial plasma response. [They had also a negligible role in the radial dynamics. However, i-n collisions can still be important for neutral dynamics, not studied here.] The recombination frequency and the plasma flux at the sheath edge S, $n_{eS}c_s$, Eq. (13), are determined from the radial model,[11] and satisfy

$$\nu_w \simeq 5.8\delta^2\nu_e. \tag{17}$$

Figure 2 shows that $R_{ion} \ll R_{en}$, so that we can write

$$\nu_e \simeq n_n R_{en} + n R_{ei}. \tag{18}$$

Non-dimensional variables are

$$\hat{u}_z = \frac{u_z}{c_s}, \quad \hat{u}_{\theta e} = \frac{u_z}{c_e}, \quad \hat{n} = \frac{n}{n_0}, \quad \hat{n}_n = \frac{n_n}{n_{n0}}, \quad \hat{z} = \frac{z}{\lambda_0}, \quad \hat{\nu}_j = \frac{\nu_j}{\nu_0}, \ (j = w, e, ...), \tag{19}$$

with $n_{n0} = g_0/u_n$, $n_0 = g_0/c_s$, $\nu_0 = R_{ion}n_{n0}$ (an ionization frequency), and $\lambda_0 = c_s/\nu_0$ (an ionization mean-free-path). Then, using an auxiliary variable ζ for regularization, the axial equations become

$$\frac{d\hat{z}}{d\zeta} = 1 - \hat{u}_z^2, \tag{20}$$

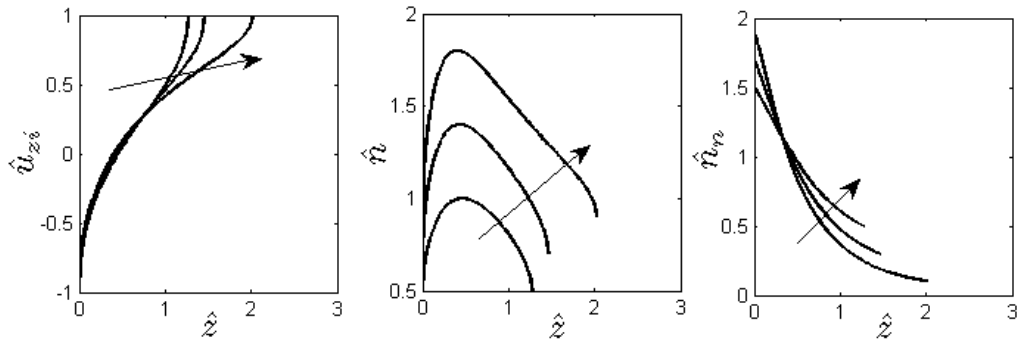

Figure 4. Axial profiles for $\alpha_{in} = 0$, $\alpha_w = 0$, and η_u =.5, 0.7 and 0.9 (increasing along the arrows).

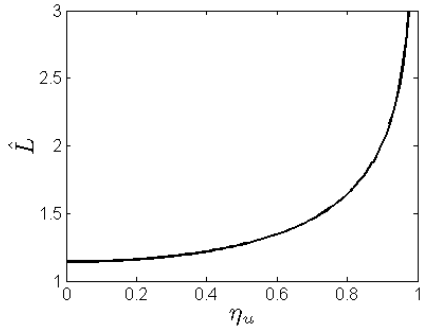

Figure 5. (a) The propellant utilization law, $\eta_u(\hat{L})$ for α_{in}=0 and α_w=0. (b) Propellant utilization versus plasma temperature for L =10cm and $n_{n0} = 10^{19}\mathrm{m}^{-3}$.

$$\frac{d\hat{u}_z}{d\zeta} = \hat{n}_n(1 + \hat{u}_z^2) - \hat{\nu}_w, \tag{21}$$

$$\frac{d\hat{n}}{d\zeta} = -\left(2\hat{n}_n - \hat{\nu}_w\right)\hat{u}_z\hat{n}, \tag{22}$$

$$\hat{n}_n = 1 - \hat{u}_z\hat{n}, \tag{23}$$

with

$$\hat{\nu}_w = a_n\hat{n}_n + a_i\hat{n}, \quad a_n = 5.8\delta^2\frac{R_{en}}{R_{ion}}, \quad a_i = 5.8\delta^2\frac{R_{ei}}{R_{ion}}\sqrt{\frac{u_n}{c_s}}. \tag{24}$$

For the values of Table 1, one has $a_n = 6.9 \cdot 10^{-3}$ and $a_i = 6.3 \cdot 10^{-3}$.

The propellant utilization, η_u, is defined as the ratio between the ion flow at exit E and the injected gas flow at A,

$$\eta_u = \dot{m}_{iE}/\dot{m}. \tag{25}$$

It turns out that $\eta_u = \hat{n}_E$. This makes convenient to use η_u as free parameter, instead of the (dimensionless) chamber length $\hat{L}$ and to integrate equations from exit E to rear wall A. The boundary conditions at E are

$$\hat{u}_z = 1, \quad \hat{n} = \eta_u, \quad \hat{n}_n = 1 - \eta_u, \tag{26}$$

and the integration ends when $\hat{u}_z = -1$.

A. Negligible losses at lateral walls

In the limit of very small losses at the lateral wall (i.e. $\hat{\nu}_w = 0$) Eqs. (20)- (23) admit a semi-analytical solution in the variable ξ defined by $d\xi/d\zeta = \hat{n}_n$. One has

$$\hat{u}_z = \tan\xi, \tag{27}$$

$$\hat{n} = 2\eta_u\cos^2\xi, \tag{28}$$

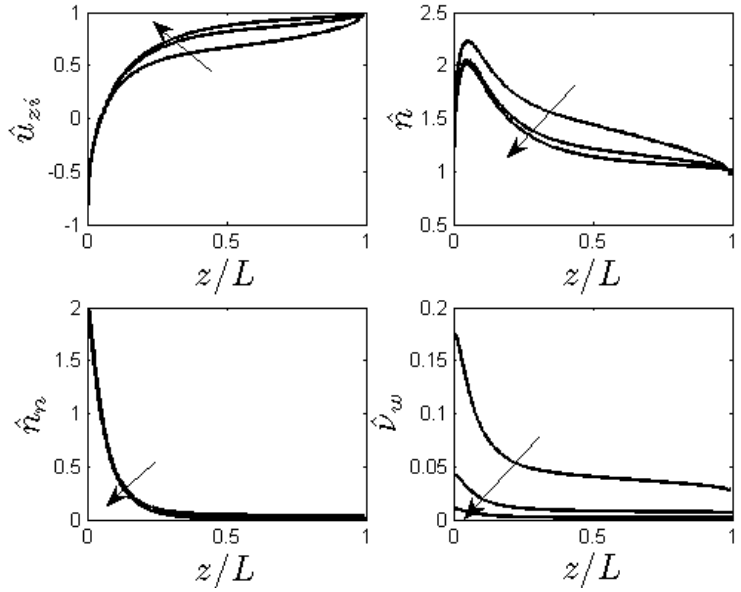

Figure 6. Axial profiles for $T_e = 15$eV and B(in Gauss)=300, 600, and 1200 (along the arrows). Rest of parameters as in Table 1.

$$\hat{n}_n = 1 - \eta_u \sin(2\xi), \tag{29}$$

$$\hat{z} = \int_{-\pi/4}^{\xi} d\xi \frac{1 - \hat{u}_z^2}{\hat{n}_n}. \tag{30}$$

The chamber ends, A and E, are at $\xi = -\pi/4$ and $\pi/4$, respectively. Some examples are shown in Fig. 4. Functions $\hat{u}_z(\xi)$ and $\hat{n}(\xi)$ are symmetric with respect to the point D (i.e. $\xi = 0$), where $\hat{u}_z = 0$, and the plasma density is maximum there, $\hat{n}_D = 2\eta_u$. However, since $\hat{z}(\xi)$ is not symmetric, the spatial profiles of $\hat{u}_z$ and $\hat{n}$ are not symmetric in the physical space with respect to the chamber mid-section; point D is closer to the rear wall, as Fig. 4 shows.

The quadrature on $\hat{z}(\xi)$ yields the propellant utilization law in the form

$$L/\lambda_0 = \hat{L}(\eta_u), \tag{31}$$

where the monotonic function $\hat{L}(\eta_u)$ is plotted in Fig. 5. One has $\hat{L} \to \pi - 2$ for $\eta_u \to 0$ and $\eta_u > 0.95$ for $\hat{L} > 3$. The propellant utilization also increases T_e or n_{n0} increase. The dependence of η_u on T_e is very drastic at low temperatures. For $T_e < 10$eV, say, η_u depends exponentially on T_e, through $R_{ion} \propto \exp(-E_{ion}/T_e)$. The influence of n_{n0} on η_u includes the dependence on the mass flow and u_n.

Figure 6 shows the plasma response when lateral losses are included. The plots show how the lateral-wall losses increase as the magnetic confinement is reduced. The main effects of lateral losses in the plasma response are to reduce n_E and to increase n_A.

IV. Current and energy balances

A. Plasma current balance

The ion currents to the rear wall S_A, the lateral wall S_W, and the chamber exit S_E are

$$I_E = I_m \eta_u, \quad I_A = I_m \hat{n}_A, \tag{32}$$

$$I_W = 2\pi R e c_s \int_0^L dz n_{eS} = I_m \int_0^{\hat{L}} d\hat{z} \hat{\nu}_w \hat{n}, \tag{33}$$

where $I_m = e\dot{m}/m_i = \pi R^2 e g_0$ is the total-ionization current (if all ions are singly-charged), based on the injected flow. The total plasma current produced in the chamber is

$$I = I_E + I_A + I_W. \tag{34}$$

If the plasma source operates efficiently and $\eta_u \approx 1$, one has

$$I_A \sim I_E \sim I_m, \quad I_W \sim I_E \times 5.8\delta^2 \frac{L\nu_e}{c_s}. \tag{35}$$

Thus, a good magnetic-confinement, leading to $I_W \ll I_E$ requires that

$$\delta^2 \ll \frac{5.8 c_s}{L\nu_e} \quad \text{i.e.} \quad \omega_{lh} \gg \frac{c_s}{R}\sqrt{\frac{L\nu_e}{c_s}}. \tag{36}$$

B. Energy balance

The plasma model is completed with the electron energy equation,

$$\nabla \cdot \left(m_e u_\theta^2/2 + 5T_e/2\right) n_e \boldsymbol{u}_e \nabla \cdot \boldsymbol{q}_e = e n_e \boldsymbol{u}_e \cdot \nabla\phi - n_e \nu_{ion} E'_{ion} + \dot{P}_a, \tag{37}$$

where $\dot{P}_a$ is the power density absorbed locally from the helicon wave, and $E'_{ion}(T_e)$ is the effective ionization energy, commented in the Appendix.

The mechanical energy equation for ions reads

$$\nabla \cdot (n_e \boldsymbol{u}_i m_i u_i^2/2) + \nabla \cdot \boldsymbol{q}_e = -e n_e \boldsymbol{u}_i \cdot \nabla\phi - \dot{P}_i, \tag{38}$$

where $\dot{P}_i = \boldsymbol{R}_i \cdot \boldsymbol{u}_i - n_e \nu_{ion} m_i u_i^2/2$ accounts for the ion energy losses. Adding this equation to Eq. (37), and taking into account that $\nabla \cdot n_e(\boldsymbol{u}_i - \boldsymbol{u}_e) = 0$ one has

$$\nabla \cdot \left[\left(\frac{m_i}{2}u_i^2 + E'_{ion}\right) n_e \boldsymbol{u}_i + \left(\frac{m_e}{2}u_\theta^2 + \frac{5}{2}T_e\right) n_e \boldsymbol{u}_e + \boldsymbol{q}_e + e\phi(n_e \boldsymbol{u}_i - n_e \boldsymbol{u}_e)\right] = \dot{P}_a - \dot{P}_i + n_e \boldsymbol{u}_i \cdot \nabla E'_{ion}. \tag{39}$$

Assuming that the two last terms on the right are small compared to $\dot{P}_a$, and setting $\boldsymbol{u}_e \simeq \boldsymbol{u}_i$, we have

$$\nabla \cdot \left[n_e \boldsymbol{u}_i \left(\frac{m_i}{2}u_i^2 + \frac{m_e}{2}u_\theta^2 + \frac{5}{2}T_e + E'_{ion}\right)\right] + \nabla \cdot \boldsymbol{q}_e = \dot{P}_a. \tag{40}$$

A global energy balance is carried out in order to determine T_e.[10] The control volume Ω for the quasineutral plasma is limited by the rear wall S_A, the lateral wall S_W, and the exit surface S_E. Notice that the Debye sheaths next to S_A and S_W do not contribute to the energy balance since they are current-free. Integrating Eq. (40) over that control volume one has

$$P_a = \int_\Omega d\Omega \dot{P}_a = P_E + P_A + P_W + P_{ion}, \tag{41}$$

where the terms on the right hand-side are the energy flows at the different surfaces and the power spent in ionization and excitation/radiation. Assuming $T_e = \text{const}$ and well-known results for a Debye sheath one has

$$P_J = 3T_e \frac{I_J}{e} + \pi c_s \int_0^R dr\ r[m_e u_\theta^2 n_e]_J, \quad J = E, A, \tag{42}$$

$$P_W = 2\pi R c_s \int_0^L dz\ n_{eS}\left(\frac{1}{2}m_i u_z^2 + \frac{1}{2}m_e u_{\theta S}^2 + \frac{5}{2}T_e + T_e \ln\sqrt{\frac{m_i}{2\pi m_e}}\right), \tag{43}$$

$$P_{ion} = E'_{ion}\frac{I}{e}. \tag{44}$$

Operating with the above expressions, the energy flow at the exit and rear-wall of the chamber are expressed as

$$P_J = \frac{I_J}{e} 3T_e \left(1 + \frac{2.3}{3}\delta^2 \int_0^{1-\delta} d\hat{r}\ \hat{r}\frac{J_1(a_0\hat{r})^2}{J_0(a_0\hat{r})}\right), \quad J = E, A, \tag{45}$$

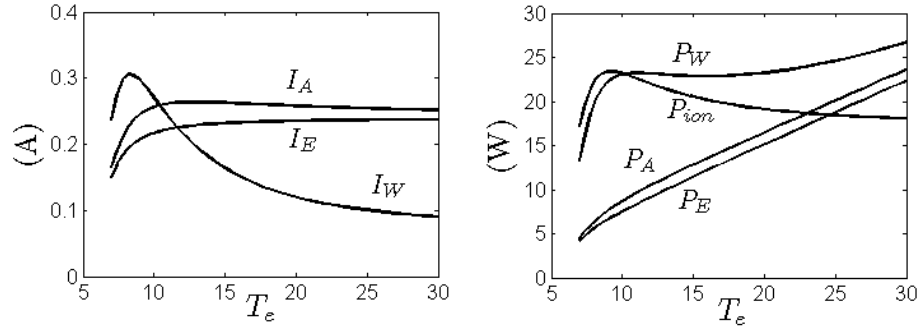

Figure 7. Plasma currents and power terms versus T_e for $B = 300$G. Rest of parameters as in Table 1.

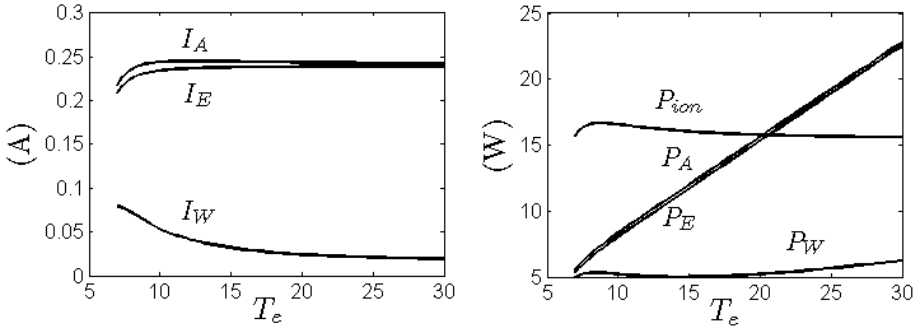

Figure 8. Plasma currents and power terms versus T_e for $B = 600$G. Rest of parameters as in Table 1.

where the second term inside the parentheses is the contribution of the electron azimuthal energy. The integral of that term is close to 1 and varies very weakly with δ, going from 1 to 2 when δ goes from 10^{-2} to 10^{-4}. Thus, there can be very good radial confinement with only a small amount of electron azimuthal energy.

The energy flow into the lateral wall is

$$P_W = \frac{I_m}{e} T_e \int_0^{\hat{L}} d\hat{z}\; \hat{n}\hat{\nu}_w \left(\frac{\hat{u}_z^2}{2} + \ln \frac{\omega_{lh}}{\nu_e} + \frac{5}{2} + \ln \sqrt{\frac{m_i}{2\pi m_e}} \right); \tag{46}$$

thus,

$$P_W \approx \frac{I_W}{e} T_e \left(\ln \frac{\omega_{lh}}{\nu_e} + \frac{5}{2} + \ln \sqrt{\frac{m_i}{2\pi m_e}} \right). \tag{47}$$

Introducing the expressions of the different power contributions into the right-hand-side of Eq. (41), an implicit equation for T_e is obtained in terms of the absorbed power, P_a, and the rest of the model parameters. It is more convenient to see Eq. (39) as an explicit equation yielding the absorbed power required to obtain a plasma with given T_e and I_m; for thruster design purposes, notice that the specific impulse is proportional to $\sqrt{T_e}$.

If lateral-wall losses can be neglected one has

$$P_a \simeq \eta_u \frac{\dot{m}}{m_i} 2 \Big[3T_e + E'_{ion}(T_e) \Big]. \tag{48}$$

Propellant utilization near to one can be easily obtained if T_e is not too low. Therefore, for a given absorbed power, there is a trade-off between the injected mass flow and the plasma temperature, which reproduces the known trade-off between thrust and specific impulse. Our plasma model depends on a too simple model for neutrals: $u_n = \text{const}$. To this respect, observe that, as long as $\eta_u \simeq 1$, the particular model of neutral dynamics is not much relevant in the main performance parameters.

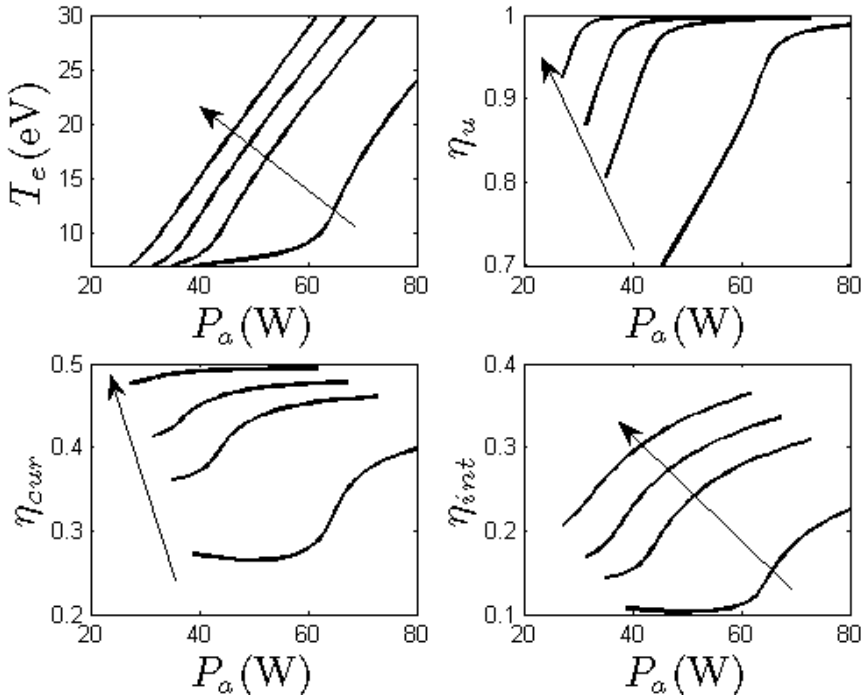

Figure 9. Plasma performances versus T_e for B(in Gauss)= 300, 450, 600, 1200 (along the arrows). Rest of parameters as in Table 1.

V. Results. Partial efficiencies

Figures (7) and (8) show the several currents and powers for the small helicon thruster of Table 1, in terms of T_e and for two values of the magnetic field. In both cases, the propellant utilization is very high for T_e >15 eV. At 300G, the plasma is weakly confined and losses to the lateral wall are very too large. At 600G, the radial confinement is already rather good. Observe that ionization losses tend to decrease with T_e increasing because of the lower ionization cost. Finally, the two figures shows the main drawback of the chamber configuration we are considering, where radial confinement can be excellent but there is no plasma confinement at the rear-wall. As a consequence, the current to the chamber black-plate is similar to the current at the chamber exit, indeed $I_A > I_E$. This back current reduces the internal efficiency of the device below a 50% and creates a high heat load in that part of the chamber.

The current efficiency is defined as the ratio of the current at the chamber exit to the total current produced in the chamber,

$$\eta_{cur} = I_E/I. \tag{49}$$

Similarly, the chamber or internal efficiency is defined as the ratio of the plasma power at the chamber exit to the absorbed wave-power,

$$\eta_{int} = P_E/P_a. \tag{50}$$

This internal efficiency is the main parameter measuring the efficiency of the chamber as part of a thruster device. It is completed with the nozzle efficiency, analyzed in a separate paper.[8] Figure (9) plots the plasma temperature and the different efficiencies versus the absorbed power for the small helicon thruster. Observe the large influence of the confining magnetic field in the internal efficiency. The propellant utilization is large except for T_e very low. In the present configuration, the current efficiency has an upper bound of 50% at the zero lateral-wall losses limit. The upper bound of the internal efficiency is

$$\eta_{int}(T_e) \approx \frac{\eta_{cur}}{1 + E'_{ion}/(3T_e)}, \approx \frac{0.5}{1 + E'_{ion}/(3T_e)}, \tag{51}$$

which illustrates the weight of ionization losses in the energy balance. The unavoidable losses decrease as T_e increases. The large effect of the ionization cost on the thruster efficiency is due to the electrothermal

character of this thruster and the limited thermal energy ($\sim 3T_e$ per ion) to be converted in beam axial energy.

VI. Conclusions

A model of 2D dynamics inside an elongated helicon plasma source with an axial magnetic field has been developed. The relevance of different physical phenomena to the plasma response has been discussed. For instance: ion-neutral collisions are found to have a negligible role in both radial and axial dynamics of the plasma; the Hall current and related azimuthal electron inertia and central phenomena in radial dynamics; and the ion azimuthal drift is negligible.

In the magnetized regime, when there plasma is well confined radially, the radial solution, which was studied in a recent work, is analytical and consists of two regions. That solution has been used to derive a model of axial dynamics. The axial response is dominated by the ionization of the injected neutral gas, the plasma heating, and the acceleration to sonic conditions of the plasma at both the chamber exit and the sheath edge formed at the rear wall.

For a thruster application the plasma temperature needs to be high, above 15 eV, say, in order to have (1) a near-total propellant utilization, (2) moderate power losses, and (3) a good specific impulse. For a given absorbed wave-power, there is a trade-off between the injected flow of neutral gas and the plasma temperature.

Efficient radial confinement are found to reduce the lateral-wall losses to a negligible value. However, the configuration we have studied provides no plasma confinement with respect to the rear wall. This means large losses there, that place the internal efficiency below a 40%. Therefore, a design modification is suggested in order to confine the plasma away of the rear wall. The creation of a magnetic mirror near the rear wall seems an efficient way to quench the losses to the rear wall.

Acknowledgments

This work was supported by the Ministerio de Ciencia e Innovación of Spain (Project ESP2007-62694) and the European Community (Grant 218862). The author thanks Prof. Martínez-Sánchez for many clarifying conversations.

A. Collision rates

The expressions proposed below for the different collision rates are reasonable approximations for the purposes of this work. The rates for ionization, electron-neutral collisions, electron-ion collisions, and ion-neutral collisions are, respectively,

$$R_{ion}(T_e) = c_e \sqrt{\frac{8}{\pi}} \sigma_{ion} \frac{1 + T_e E_{ion}}{(T_e + E_{ion})^2} \exp\left(-\frac{E_{ion}}{T_e}\right), \tag{52}$$

$$R_{en}(T_e) = \sqrt{\frac{8T_e}{\pi m_e}} \sigma_{en}, \tag{53}$$

$$R_{ei}(T_e, n_e) = \left(\frac{T_e}{1\ \mathrm{eV}}\right)^{-3/2} \frac{\ln \Lambda(T_e, n_e)}{10} \cdot 9.2 \cdot 10^{-13} \mathrm{m^3 s^{-1}}, \tag{54}$$

with E_{ion} the first ionization energy. For ion-neutral collisions, we have

$$R_{in}(c_{in}) = c_{in}(k_2 - k_1 \log_{10} c_{in})^2 \qquad [50] \tag{55}$$

with $c_{in} = |\boldsymbol{u}_i - \boldsymbol{u}_n|$, that we prefer to express as

$$R_{in}(c_{in}) = R_{ins}(T_e) \hat{c}_{in} (1 - a_1 \log_{10} \hat{c}_{in})^2, \tag{56}$$

with $\hat{c}_{in} = c_{in}/c_s$, $R_{ins} = R_{in}(c_s)$, and $a_1 = k_1(k_2 - k_1 \log_{10} c_s)^{-1}$. The constants involved in the above expressions depend on the injected gas. For argon, we used $E_{ion} = 15.76\mathrm{eV}$, $\sigma_{ion} = 2.8 \cdot 10^{-20}\mathrm{m}^2$, $\sigma_{en} = 15 \cdot 10^{-20}\mathrm{m}^2$, $k_2 = 10.5 \cdot 10^{-10}\mathrm{m}$, and $k_1 = 1.67 \cdot 10^{-10}\mathrm{m}$.

For T_e = const and a given gas, R_{ion}, R_{en}, and R_{ins} are constant; R_{ei} is a constant too if an average value is used for $\ln\Lambda(n_e, T_e)$. Observe that the non-linear expression used for R_{in}, Eq. (55), correspond to the high-pressure case of Fruchtman et al.[10] In spite of it, i-n collisional effects will be found negligible in the desired operation range.

Excitation collisions are taken into account through the effective ionization energy $E'_{ion}(T_e) = E_{ion}\alpha_{ion}(T_e)$ and α_{ion} the ionization cost factor. From Dugan,[16] a fitting formula for argon is

$$\alpha_{ion}(T_e) \approx 1.4 + 0.4\exp(0.7\ E_{ion}/T_e). \tag{57}$$

References

[1]T. Ziemba, J. Carscadden, J. Slough, J. Prager, and R. Winglee, High Power Helicon Thruster, in *41th Joint Propulsion Conference, Tucson, AR*, AIAA 2005-4119, American Institute of Aeronautics and Astronautics, Washington DC, 2005.

[2]O. Batishchev, IEEE Transaction on Plasma Science **37**, 1563 (2009).

[3]R. Boswell and F. Chen, IEEE Transactions on Plasma Science **25**, 1229 (1997).

[4]S. M. Tysk, C. M. D. J. E. Scharer, and K. Akhtar, Physics of Plasmas **11**, 878 (2004).

[5]J. Gilland, R. Breun, and N. Hershkowitz, Plasma Sources Sci. Technol. **7**, 416 (1998).

[6]S. Cho and M. Lieberman, Physics of Plasmas **10**, 882 (2003).

[7]E. Ahedo and M. Merino, Two-dimensional plasma acceleration in a divergent magnetic nozzle, in *44th Joint Propulsion Conference, Hartford, CT*, AIAA 2009-5361, American Institute of Aeronautics and Astronautics, Washington DC, 2008.

[8]E. Ahedo and M. Merino, in *31th International Electric Propulsion Conference, Ann Arbor, Michigan, USA*, IEPC 2009-002, Electric Rocket Propulsion Society, Fairview Park, OH, 2009.

[9]E. Ahedo, J. Gallardo, and M. Martínez-Sánchez, Physics of Plasmas **10**, 3397 (2003).

[10]A. Fruchtman, G. Makrinich, and J. Ashkenazy, Plasma Sources Science and Technology **14**, 152 (2005).

[11]E. Ahedo, 'Parametric analysis of a magnetized cylindrical plasma', submitted to Physics of Plasmas (2009).

[12]L. Tonks, Physical Review **56**, 360 (1939).

[13]H. Ewald, F. Crawford, and S. Self, Journal of Applied Physics **38**, 2753 (1967).

[14]N. Sternberg, V. Godyak, and D. Hoffman, Physics of Plasmas **13**, 063511 (2006).

[15]D. Pavarin et al., Design of 50W Helicon Plasma Thruster, in *31th International Electric Propulsion Conference, Ann Arbor, Michigan, USA*, IEPC 2009-205, Electric Rocket Propulsion Society, Fairview Park, OH, 2009.

[16]J. Dugan and R. Sovie, Volume ion production costs in tenuous plasmas: A general atom theory and detailed results for helium, argon, and cesium, Technical report, NASA TN D-4150, 1967.